Integral Formulation and Genetic Algorithms for Defects Geometry Reconstruction Using Pulse Eddy Currents

Gabriel Preda, Mihai Rebican, and Florea Ioan Hantila

Electrical Engineering Department, Politehnica University of Bucharest, Bucharest 060042, Romania

A method for reconstruction of zero-thickness defects, buried deep under material surface, using pulse eddy currents, is proposed. Both an integral-FEM method for simulation of transient eddy-currents and genetic algorithms, as a model-free inversion technique, are proposed. Numerical results for the inversion of the eddy-currents signals, using genetic algorithms, are shown.

***Index Terms*—Crack detection, eddy current testing, genetic algorithms.**

I. Introduction

PULSE eddy currents technique is proposed as a method to detect cracks in conductive materials with large thickness. For thin structures, Eddy Currents Testing (ECT) using harmonic mode was used extensively in the past for detection of cracks in steam generator (SG) tubing of pressurized water reactors (PWR) of nuclear power plants. Although its advantages, as high speed and reliability for the routine inspections, skin effect limits this method only to thin and nonmagnetic structures. Pulse eddy currents have multiple advantages: the rectangular pulse profile accounts for a multi-frequency analysis, the lower harmonics penetrating deeper in the material, while limiting the heating exposure of the coil-probe system to only the short duration of a signal allows an increase in the power [1], [2]. Multiple industrial applications were reported, such as detection of cracks in multiple layered plates around fasteners for aeronautics industry [3], crack detection and thickness and conductivity evaluation in structural steels [4].

Reconstruction of crack shape from scanned signals requires the solution of an inverse problem and involves the calculation of a large number of forward problems. Implementation of a fast and accurate direct solver is therefore critical for achieving a rapid solution of the inverse problem. Several solutions were proposed in literature, for fast solution of eddy-currents computation using integral methods [5], [6].

For defects with zero-thickness in conductive plates, a method combining fast solution of the forward problem and genetic algorithms for the inverse problem was proposed in [7]. The forward problem can be reformulated as the determination of the modified eddy current pattern due to the presence of the defect [8], [9]. Calculation of only the perturbed signal makes possible that, when generating the solution corresponding to a candidate flaw only a very small part of the whole matrix describing the full model must be inverted [7], [9].

Both problem-dependent methods, like gradient-descent [10] and problem-free, artificial inteligence-based methods, like genetic algorithms [8], tabu search [11] or neural networks [4], [12] were proposed for the solution of inverse problems.

In the current study we investigate the possibility to reconstruct geometry of zero-thickness defects using simulated pulse eddy currents signals and an inversion procedure based on a parallel implementation of genetic algorithms.

II. Formulation for the Forward Problem

The proposed method is based on application of $\mathbf{T}$—electric vector potential to the integral equation of eddy currents, like in [13]. Starting from Maxwell equations in quasi-stationary form and the constitutive relationship

$$\boldsymbol{E} = \rho \cdot \boldsymbol{J} \tag{1}$$

where $\boldsymbol{J}$ is the current density, $\boldsymbol{E}$ is the electrical field and ρ is the resistivity in the conductive domain Ω_c. In the specimen coordinates frame, the electrical field is

$$\mathbf{E} = -\frac{\partial \mathbf{A}}{\partial t} - \nabla V \tag{2}$$

where V is the electric scalar potential and $\boldsymbol{A}$ is magnetic vector potential. The magnetic vector potential can be calculated using Biot–Savart formula

$$\mathbf{A} = \frac{\mu_0}{4\pi} \int_{\Omega} \frac{\mathbf{J}}{r} \mathrm{d}v + \mathbf{A}_0 \tag{3}$$

with $\mathbf{A}_0$ being the magnetic vector potential due to the impressed current sources

$$\mathbf{A}_0 = \frac{\mu_0}{4\pi} \int_{\Omega_0} \frac{\mathbf{J}_0}{r} \mathrm{d}v \tag{4}$$

and Ω_0 being the air. Only conductive media are meshed. The current density is expressed in terms of shape functions associated to the edges in the inner co-tree [13]

$$\mathbf{J} = \sum_{k=1}^{n} N_k \nabla \times \mathbf{T}_k. \tag{5}$$

Manuscript received December 13, 2009; revised February 14, 2010; accepted February 18, 2010. Current version published July 21, 2010. Corresponding author: G. Preda (e-mail: preda@elth.pub.ro; gabi.preda@gmail.com).

Digital Object Identifier 10.1109/TMAG.2010.2044143

Applying Galerkin approach, the following equation system is obtained:

$$[R]\{I\} + [L]\frac{d\{I\}}{dt} = \{U\} \tag{6}$$

where the terms of matrices $[\boldsymbol{R}]$ and $[\boldsymbol{L}]$ and the right-hand term $\{U\}$ are

$$L_{ij} = \frac{\mu_0}{4\pi}\int\limits_{\Omega_c}\int\limits_{\Omega_c}\frac{\nabla\times\mathbf{T}_i\cdot\nabla\times\mathbf{T}_j}{r}dv_c dv_c, \tag{7}$$

$$R_{ij} = \int\limits_{\Omega_c}\nabla\times\mathbf{T}_i\cdot\rho\nabla\times\mathbf{T}_j dv_c, \tag{8}$$

$$U_i = -\frac{\partial}{\partial t}\left(\frac{\mu_0}{4\pi}\int\limits_{\Omega_c}\int\limits_{\Omega_0}\frac{\nabla\times\mathbf{T}_i\cdot\mathbf{J}_0}{r}dv_c dv_0\right), \tag{9}$$

and the unknowns term is

$$\{I\} = \begin{bmatrix}\alpha_1\\ \alpha_2\\ \vdots\\ \alpha_N\end{bmatrix}. \tag{10}$$

In order to model 2D, zero-thickness defects, several procedures were proposed in literature. From the set of edges in the inner co-tree are eliminated, in our approach, the edges placed in the defect surface. The procedure is equivalent to zeroing the circulation of scalar electric potential $\mathbf{T}$ on those co-tree edges [7], [14].

For time integration of (6) we apply a Crank-Nicholson procedure with $\Theta = 1/2$. The time step is adapted to each particular problem, in order to simulate accurately the fast variable transient regime of pulse eddy currents. All the coefficients in the system matrix are unchanged through time integration and, therefore, the resulting matrix system is formed and inverted only once for one forward problem. In the calculation of double integral in (7), we perform the CPU intensive double integral calculation only once for the entire forward problems set, since only the co-tree is changing, not the volume mesh or the tree. This results in considerable speed-up of overall computational process.

III. Simulation Setup and Forward Problem Analysis

The simulation setup for the test problem consists in a conductive plate, a pancake coil used to energize the specimen and a Hall sensor to pick-up the signal. The pancake coil—Hall sensor system is less sensitive to frequency variation than the classical auto-induction pancake used in AC testing, which in turn can be optimized for a single frequency; for pulse excitation, such an optimization is not possible [1], [2], [4].

The test specimen is a plate made from a non-magnetic, stainless steel material. The excitation coil is a pancake shaped coil, with a pulse excitation. The plate dimensions and conductivity, the coil geometry and excitation pulse are given in Table I. The pickup sensor measures the vertical component of magnetic flux density and is placed in the coil axis, at $z = 0.4$ mm. A number of 55 time steps are simulated for a single pulse.

TABLE I
Simulation Setup: Test Specimen, Excitation Coil (Coil Geometry and Excitation Signal), and Flaw Geometry

Item	Parameter	Value
Pancake coil	Inner radius (R_{min})	2 mm
	Outer radius (R_{max})	5 mm
	Length (l)	4 mm
	Liftoff (z)	0.4 mm
Excitation pulse	I_{max}	2000 AT
	Pulse shape	trapezoidal
	Pulse duration	70 μs, 10 μs rise and fall
Test specimen	Conductivity	10^6 S/m
	Thickness	10 mm
	Dimensions	16 cm × 16 cm
Flaw	Depth	40%-80% (OD)
	Length	5-15 mm
	Thickness	0 mm (2D)

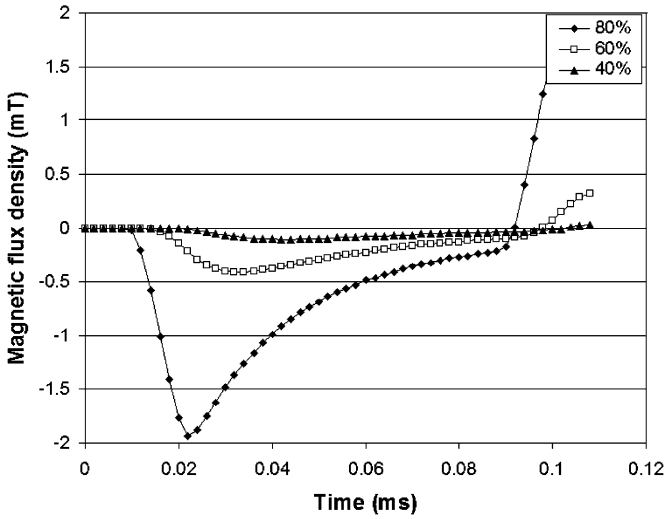

Fig. 1. Difference signals plotted against time. Defects are with zero-thickness, 12 mm long, open on outer side, ranged from 40% to 80%. The signal is the z-component of magnetic flux density, at 0.4 mm over the plate.

In Fig. 1 we show the difference between signal with crack and signal without crack (difference signal) of z-component of magnetic flux density, measured at $\mathrm{x} = 0$, $\mathrm{y} = 0$, $\mathrm{z} = 0.4$ mm (centered over the plate) for a 15 mm length, 40%, 60% and 80% outer defect (OD), with 0-thickness. The peak of the difference signal is obtained earlier for larger defects (80%) and at a later moment for the smaller defects (40%). Selecting the sampling moment according to this observation, we can increase the method sensitivity to one specific class of defects [4].

For 80% OD, with 0-thickness and with length 5, 10 and 15 mm, the difference signals measured at $\mathrm{x} = 0$, $\mathrm{y} = 0$, $\mathrm{z} = 0.4$ mm are shown in Fig. 2. Whilst the peak position in time of the difference signal is reached at 0.22 μs for all cases of 80% depth outer defects, the signal amplitude increases with the defect length.

In Fig. 3 we present the scan signal from -10 mm to 10 mm over a 15 mm long OD crack, comparing difference signals for crack depths 80%, 60% and 40%; sample moment is selected for each crack depth in order to show the maximum difference signal.

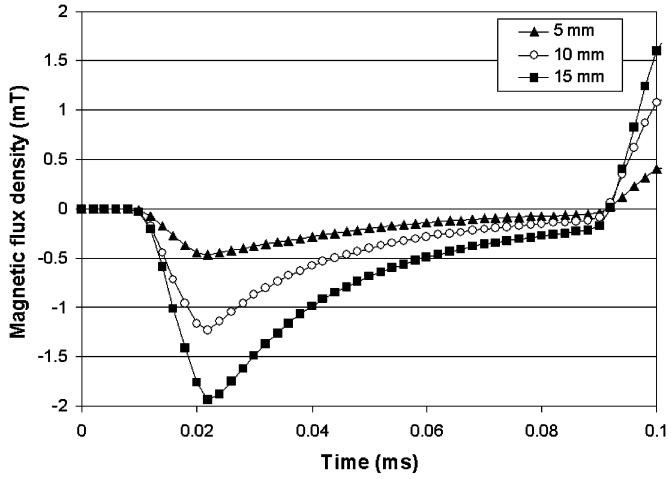

Fig. 2. Difference signal (magnetic flux density—z component) versus time; outer defects OD 80%, with 5, 10 and 15 mm length; scan point is $y = 0.0$ mm.

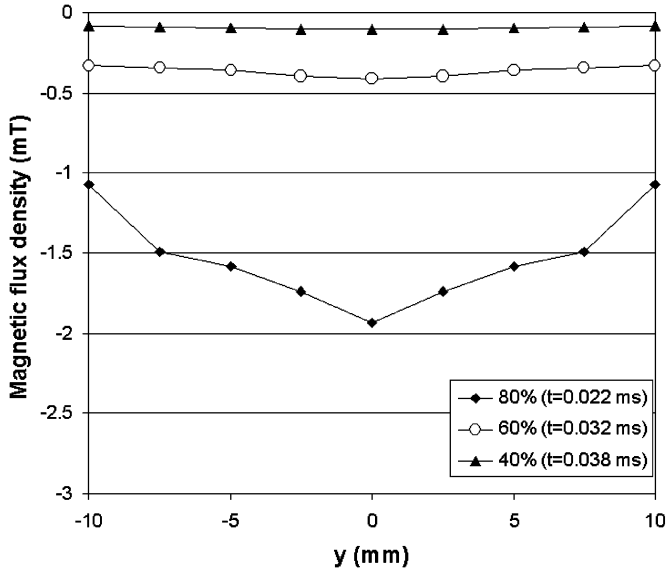

Fig. 3. Scan from −10 mm to 10 mm over a 15 mm long OD crack, comparison of difference signals of magnetic flux density for crack depths 80%, 60% and 40%; sample moment is selected for each crack depth in order to show the maximum difference signal.

IV. Inversion Procedure Using Genetic Algorithms

The scan signals are used as input in the inverse problem, for estimation of the defect geometry. The defect geometry is described by a set of parameters, one parameter for each column of cells along the scan path in the zone where we estimate there is a flaw. Each cell is 2.0 mm height and 2.5 mm length (along the scan path). The parameter value is the ratio of the depth of the crack at the corresponding location, from the full thickness of the specimen. Parameter values range from 0 to 1 (0 for no-crack, 1 for full, 100% crack). For example, for the crack described in Fig. 4, the value of parameters are: 0.4, 0.6, 0.2, 0.0, 0.8, and 0.0.

A genetic algorithm first presented in [15] is used to solve the inverse problem of inferring the geometry and position of

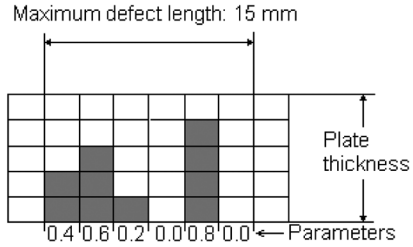

Fig. 4. Defect parameter. White color means base material, dark gray color means vanished conductivity. The value of parameter is the depth of crack at the corresponding location, as a ratio from full plate thickness.

a zero-thickness outer defect. The entry parameters for the genetic algorithm are the geometry parameters of the defect, as described in Fig. 4. The fitness function f is defined as

$$f = \sqrt{1/n_{sp} \cdot \sum_{i=1,n_{sp}} \frac{\left(\mathbf{B}^i_{z(estimated)} - \mathbf{B}^i_{z(original)}\right)^2}{\left(\mathbf{B}^i_{z(estimated)}\right)^2}} \tag{11}$$

where n_{sp} is the number of scan points, $\mathbf{B}^i_{z(original)}$ is the signal of the defect that must be reconstructed and $\mathbf{B}^i_{z(estimated)}$ is the signal for the current estimation. Minimization of f will result in a set of geometry parameters for the defect that approximate the real defect.

Each chromosome corresponds to one parameter to be evaluated, like in [15]. The chromosome length is correlated to the parameters variation space. In *pikaia* implementation, all entry parameters should range between 0 and 1 and therefore real geometric parameters must be scaled [15], [16], a chromosome segment is associated with a parameter and the chromosome length is equal to the number of digits used for representation of parameters. The following options for the genetic algorithm are set: uniform variable mutation mode, mutation rate varying between 0.0005 and 0.25, crossover probability 0.85, and reproduction plan: full generational replacement.

In the set of tests performed, each individual in the population is modeled with 6 chromosome segments (one for each parameter to be reconstructed), with a dimension of 4 bits per chromosome (that allows us to model discrete values from 0 to 1 with a 0.1 resolution; we further limit the variation to a 0.2 resolution, corresponding to the mesh size). The sampling moment for pick-up signal was selected at $t = 0.22$ μs, in order to maximize sensitivity to defects with the largest thickness. After several tests, we decided to use a population with 24 individuals evolving over a maximum of 20 generations.

In order to speed-up the numerical solution, the parallel version implementation of genetic algorithm, using Message Passing Interface (MPI), available at [17] is adopted. In this approach, the calculations of fitness function values are distributed by the master process to the available processing nodes. When a node becomes free again, it will receive a new set of calculation data, corresponding to one forward problem, for the evaluation of one fitness function. Data traffic between nodes is minimal, since only defect parameters are passed to each node and only fitness function value are returned to the master. The speed-up due to parallel computation increases linearly with the

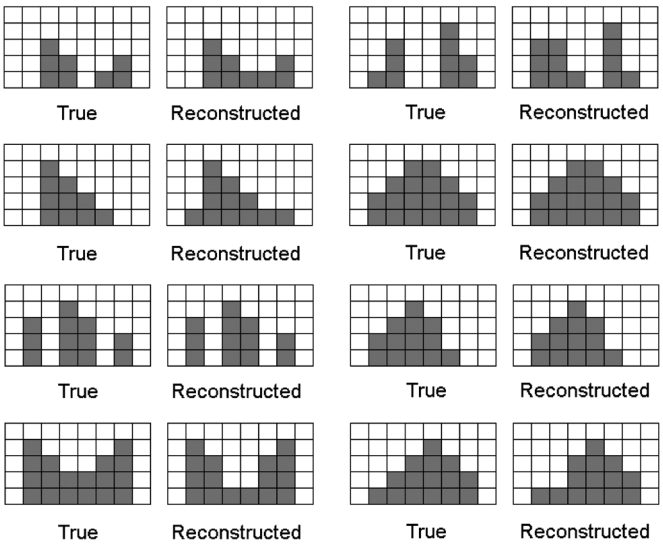

Fig. 5. Original (true) and reconstructed geometry using the genetic algorithms based inversion procedure.

number of processors, synchronization bottleneck and network lag being insignificant for this intrinsically parallel algorithm.

For the current simulations, we used a 4 CPU Intel Xeon computer with 2.8 GHz clock speed and 16 GB RAM, powered with Linux operating system. An average of 80 seconds per direct simulation is achieved.

In Fig. 5 are presented the results of inversion of simulated signals, for 8 different geometries of defect. From the original signal, the reference signal was jittered, using white noise 10% from difference signal. For each defect, two images are presented, one, in the left side, showing the true, original geometry of the defect, in the right, the reconstructed geometry using the inversion procedure.

The inversion procedure is less efficient when applied to reconstruction of defects with smaller thickness. This is because the sampling moment was selected in order to maximize the sensibility for larger, deeper defects. In most of the cases analyzed, we can observe that the geometry reconstructions are rather fair and in some cases the original and estimated geometry are identical.

V. Conclusion

Using a FEM-Integral formulation, zero-thickness flaws can be simulated by zeroing the circulation of electric vector potential in the surfaces of mesh cells that define the crack. Cracks deeper buried under surface results not only in smaller amplitude difference signals but also in delayed peak of difference signal in comparison with cracks closer to surface. Genetic algorithms were proven to be an effective method for solution of the inverse problem consisting in flaw shape and position estimation, from scanned eddy-currents induced signals.

References

[1] M. Gibbs and J. Campbell, "Pulsed eddy current inspection of cracks under installed fasteners," *Mater. Eval.*, vol. 46, pp. 51–59, 1991.

[2] J. Bowler and M. Johnson, "Pulsed eddy-current response to a conducting half space," *IEEE Trans. Magn.*, vol. 33, pp. 2258–2264, 1997.

[3] B. Lebrun, Y. Jayet, and J.-C. Baboux, "Pulsed eddy-current signal analysis: Application to the experimental detection and characterization of deep flaw in highly conductive materials," *NDT&E Int.*, vol. 30, no. 3, pp. 163–170, 1997.

[4] G. Preda, B. Cranganu-Cretu, F. I. Hantila, O. Mihalache, and K. Miya, "Nonlinear FEM-BEM formulation and model-free inversion procedure for reconstruction of cracks using eddy currents," *IEEE Trans. Magn.*, vol. 38, no. 2, pp. 1241–1244, 2002.

[5] G. Rubinacci, A. Tamburrino, S. Ventre, and F. Villone, "Fast computational methods for large-scale eddy-current computation," *IEEE Trans. Magn.*, vol. 38, no. 2, pp. 529–532, 2001.

[6] G. Rubinacci, A. Tamburrino, S. Ventre, and F. Villone, "A fast algorithm for solving 3-D eddy current problems with integral formulation," *IEEE Trans. Magn.*, vol. 37, no. 5, pp. 3099–3103, 2001.

[7] R. Albanese, G. Rubinacci, and F. Villone, "An integral computational model for crack simulation and detection via eddy currents," *J. Comp. Phys.*, vol. 152, pp. 736–755, 1999.

[8] R. Albanese, G. Rubinacci, A. Tamburrino, and F. Villone, "Non destructive evaluation in the time domain," *COMPEL*, vol. 18, no. 3, pp. 422–435, 1999.

[9] M. Morozov, G. Rubinacci, A. Tamburrino, and S. Ventre, "Numerical models of volumetric insulating cracks in eddy-current testing with experimental validation," *IEEE Trans. Magn.*, vol. 42, no. 5, pp. 1568–1576, 2006.

[10] Z. Chen and K. Miya, "ECT inversion using a knowledge based forward solver," *J. Nondestr. Eval.*, vol. 17, no. 3, pp. 157–165, 1998.

[11] M. Rebican, Z. Chen, N. Yusa, L. Janousek, and K. Miya, "Shape reconstruction of multiple cracks from ECT signals by means of a stochastic method," *IEEE Trans. Magn.*, vol. 42, no. 4, pp. 1079–1082, 2006.

[12] R. C. Popa and K. Miya, "Approximate inverse mapping in ECT, based on aperture shifting and neural network regression," *J. Nondestr. Eval.*, vol. 17, no. 4, pp. 209–221, 1998.

[13] R. Albanese and G. Rubinacci, "Integral formulation for 3D eddy current computation using edge elements," *IEE Proc.*, vol. 135, no. 7, pt. A, pp. 457–462, 1988.

[14] G. Preda, F. I. Hantila, and M. Rebican, "Eddy current solver for nondestructive testing using an integral-FEM approach and zero-thickness flaw model," in *Proc. 13th Biennial IEEE Conf. Electromagnetic Field Computation, CEFC 2008*, Athens, Greece, 2008, p. 98.

[15] P. Charbonneau, "Genetic algorithms in astronomy and astrophysics," *Astrophys. J. (Supplements)*, vol. 101, pp. 309–334, 1995.

[16] B. Cranganu-Cretu, G. Preda, O. Mihalache, Z. Chen, and K. Miya, "B-H curve reconstruction from MFL signals based on genetic algorithms," *Appl. Electromagn. Mechan.*, vol. 15, pp. 283–289, 2002.

[17] Parallel Pikaia Homepage. [Online]. Available: http://whitedwarf.org/parallel/